Supporting Information

Sub-20 nm Carbon Nanoparticles with Expanded Interlayer Spacing for High-Performance Potassium Storage

Qingmeng Gan[†‡], *Jiwei Xie*[‡], *Youhuan Zhu*[‡], *Fangchang Zhang*[‡], *Peisen Zhang*[§], *Zhen He**[†], *Suqin Liu**[†]

[†]College of Chemistry and Chemical Engineering, Hunan Provincial Key Laboratory of Chemical Power Sources, Central South University, Changsha, Hunan 410083, P. R. China

[‡]Department of Materials Science and Engineering, South University of Science and Technology of China, Shenzhen, Guangdong 518055, P. R. China.

[§]Key Laboratory of Colloid, Interface and Chemical Thermodynamics, CAS Research/Education Center for Excellence in Molecular Sciences, Institute of Chemistry, Chinese Academy of Sciences, Beijing 100190, P. R. China.

*Corresponding authors e-mails: zhenhe@csu.edu.cn (Zhen He), sqliu2003@126.com (Suqin Liu)

This 13-page file includes:

Figure S1 to S9

Table S1 and S2

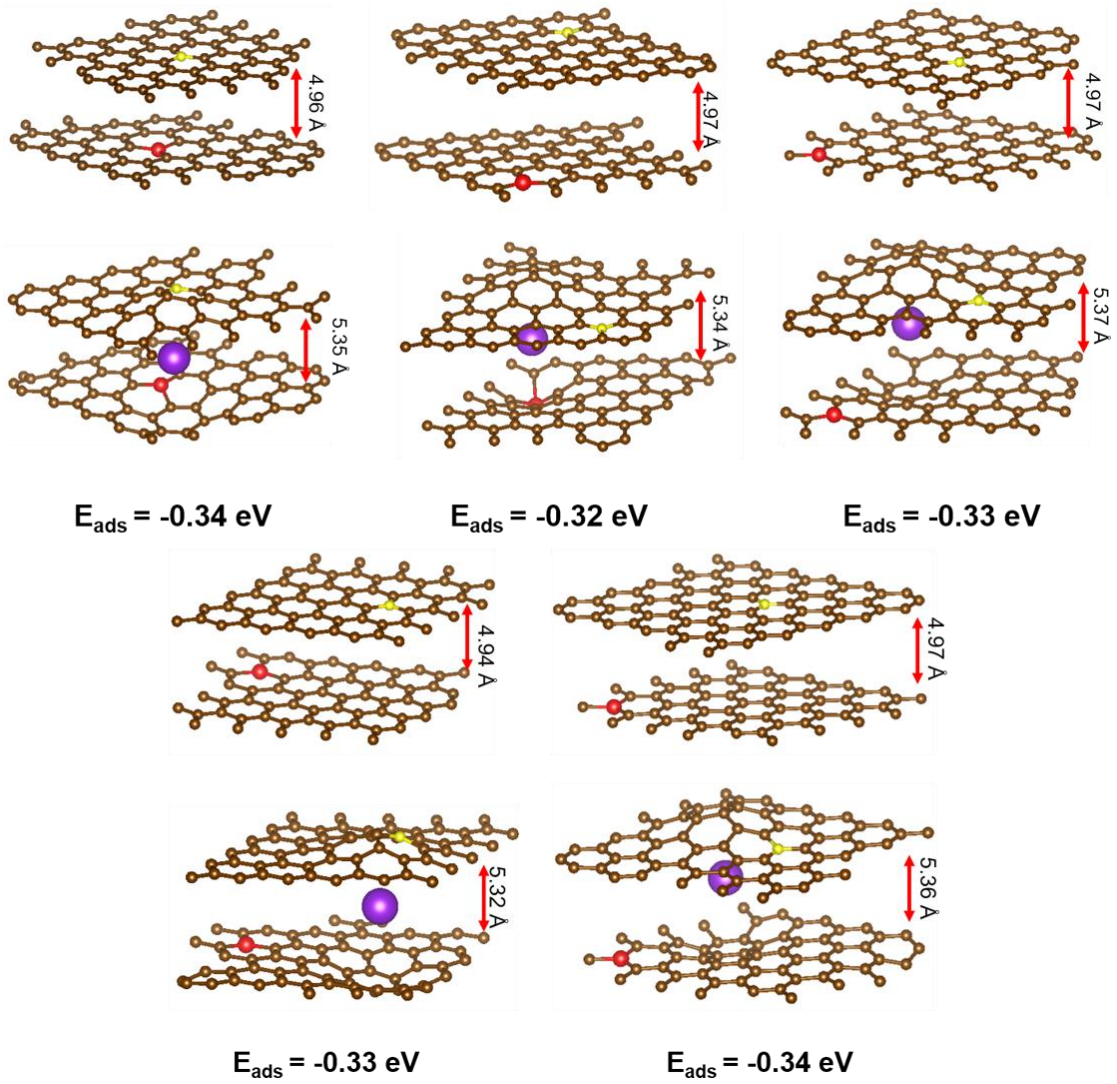

Figure S1. Graphical illustration of N and P doping sites with different relative positions with the change of interlayer distance of the N/P-codoped carbon.

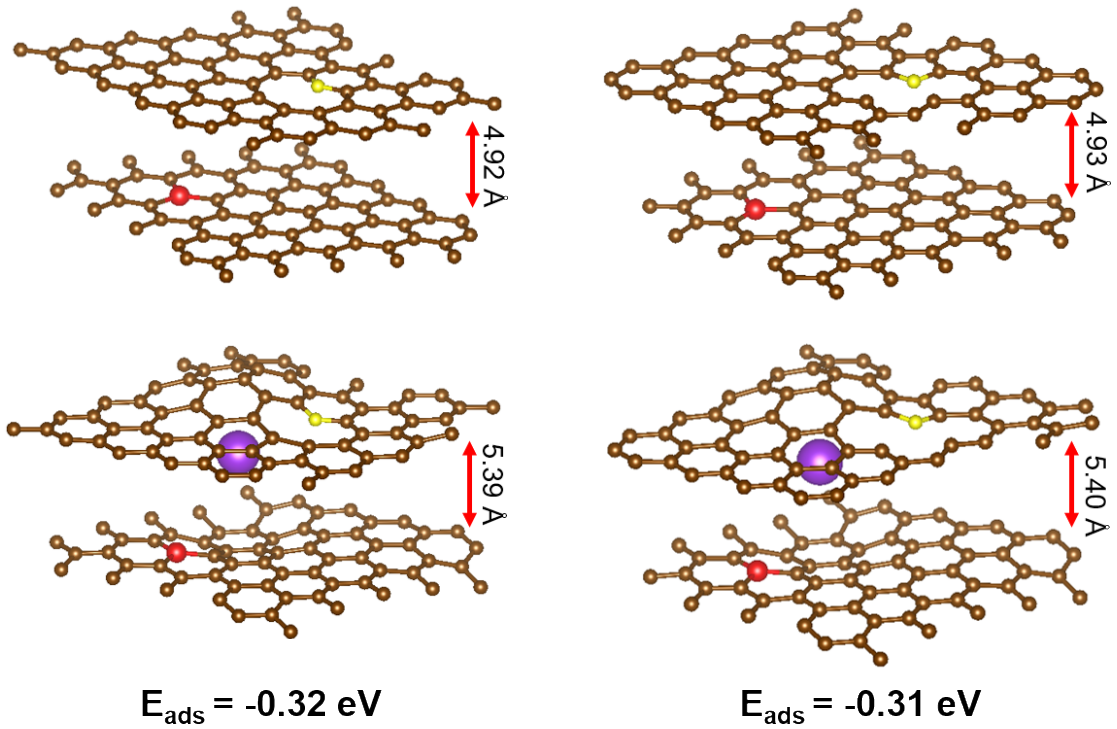

Figure S2. Graphical illustration of the doped N with different forms with the change of interlayer distance of the N/P-codoped carbon.

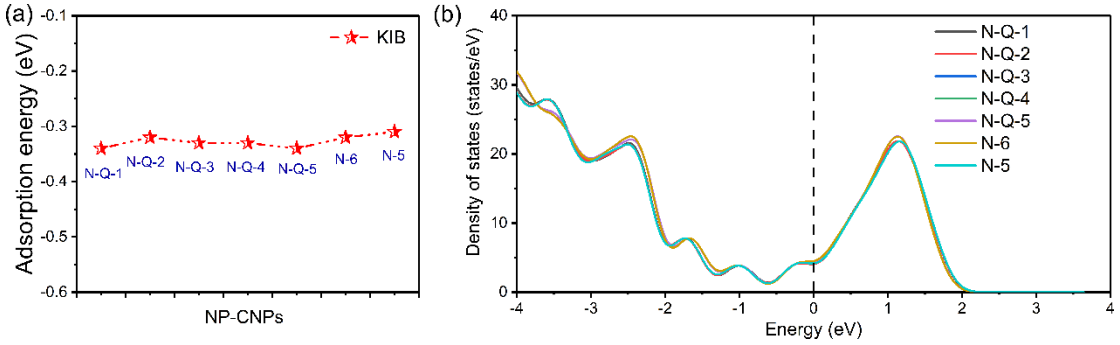

Figure S3. (a) Adsorption energy of K ions on NP-CNPs with different forms of N dopants. (b) Density of states of NP-CNPs with different forms of N dopants.

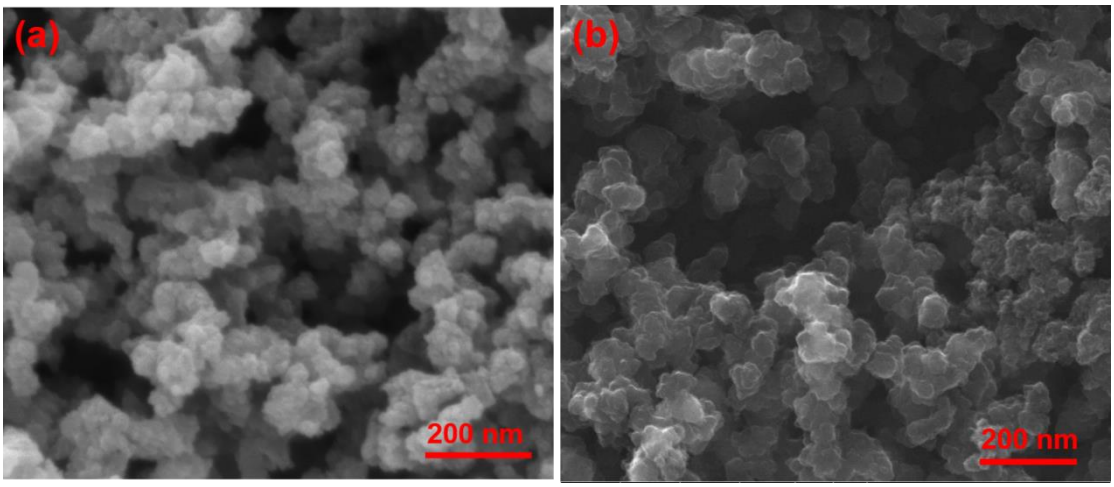

Figure S4. SEM images of (a) N-CNPs and (b) NP-CNPs.

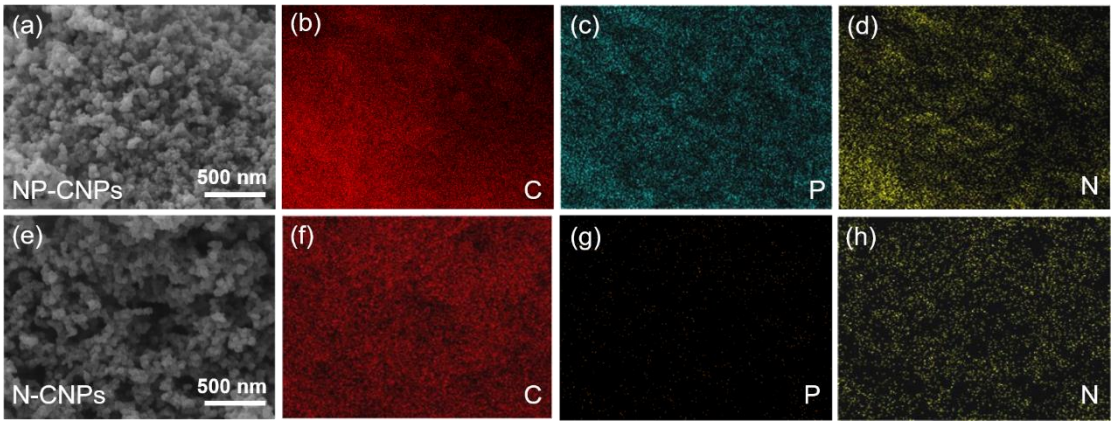

Figure S5. SEM images of (a) NP-CNPs and (e) N-CNPs and the corresponding elemental mapping images of (b) C, (c) P, (d) N for NP-CNPs and (f) C, (g) P, (h) N for N-CNPs.

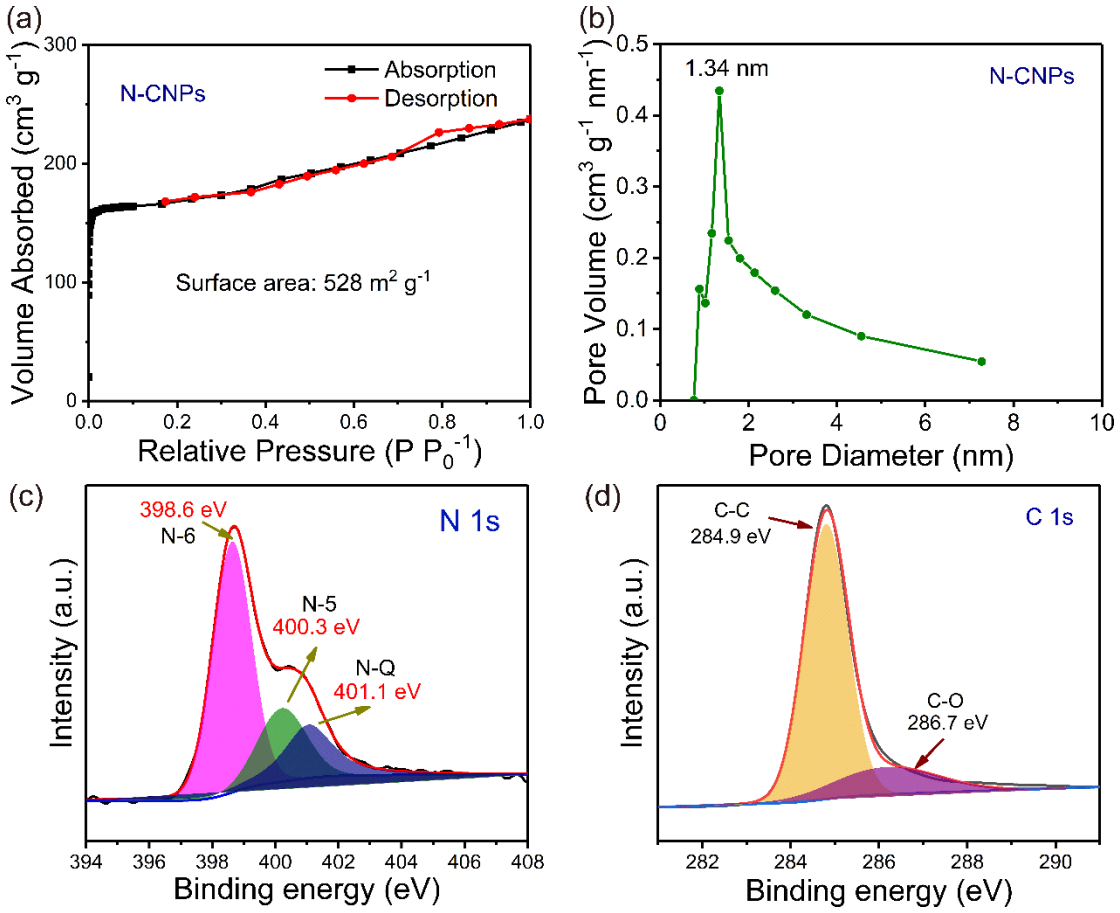

Figure S6. (a) Nitrogen absorption/desorption isotherms and (b) the corresponding pore size distribution of N-CNPs. High-resolution XPS spectra of (c) N 1s and (d) C 1s for N-CNPs.

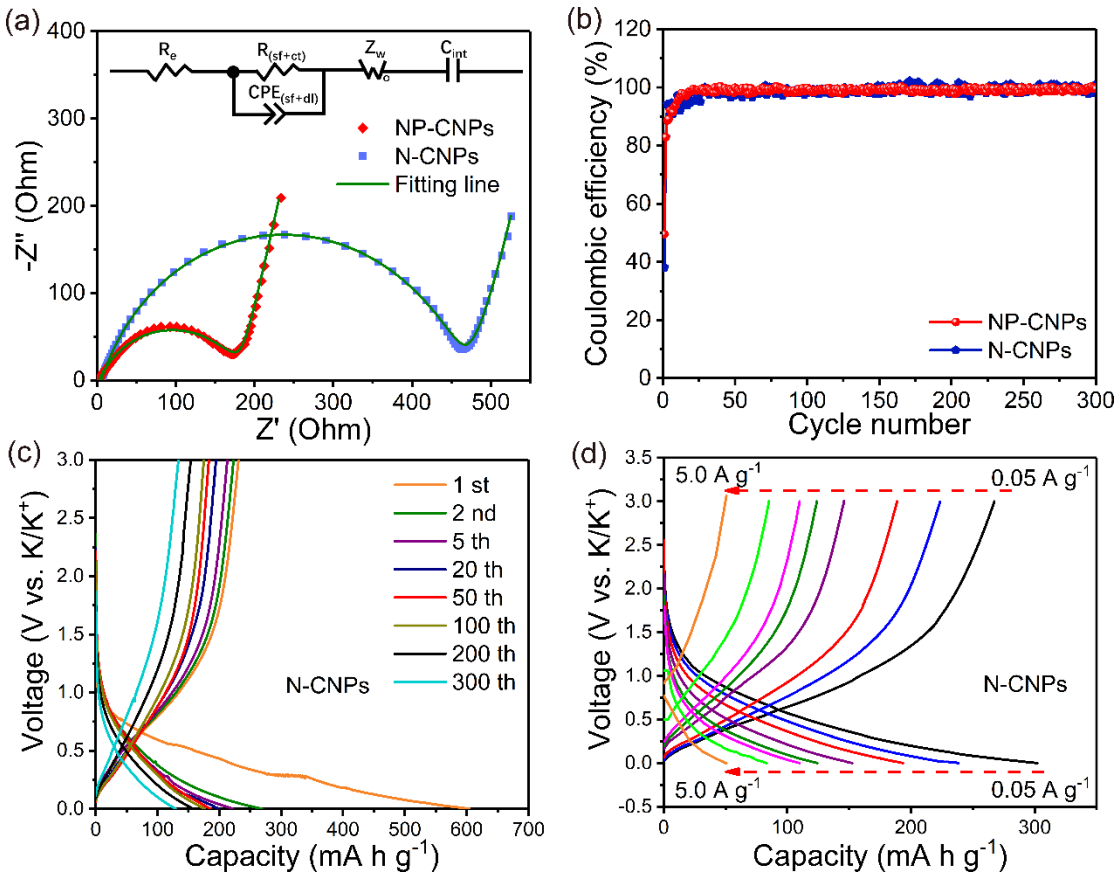

Figure S7. (a) Electrochemical impedance spectra of the N-CNPs and NP-CNPs electrodes after 10 cycles at a rate of 200 mA g^{-1}. (b) Coulombic efficiencies of the N-CNPs and NP-CNPs electrodes at 200 mA g^{-1}. (c) Galvanostatic charge and discharge voltage profiles for N-CNPs and NP-CNPs of various cycles at the rate of 200 mA g^{-1}. (d) Galvanostatic charge and discharge voltage profiles for N-CNPs and NP-CNPs at various rates.

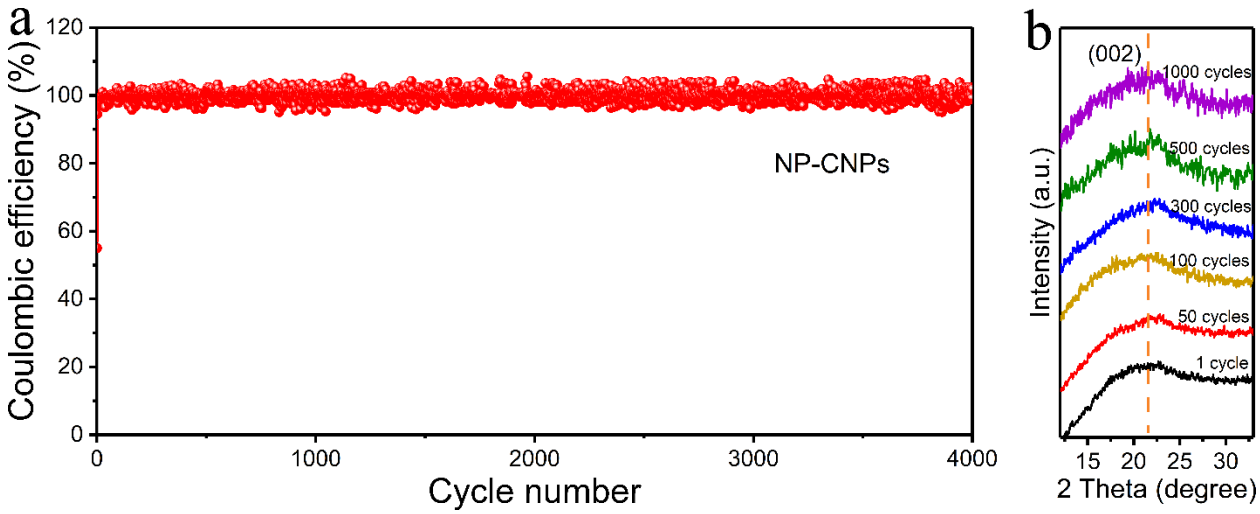

Figure S8. (a) Coulombic efficiencies of NP-CNPs electrodes at 1 A g^{-1}. (b) XRD patterns of NP-CNPs during cycling at 1 A g^{-1}.

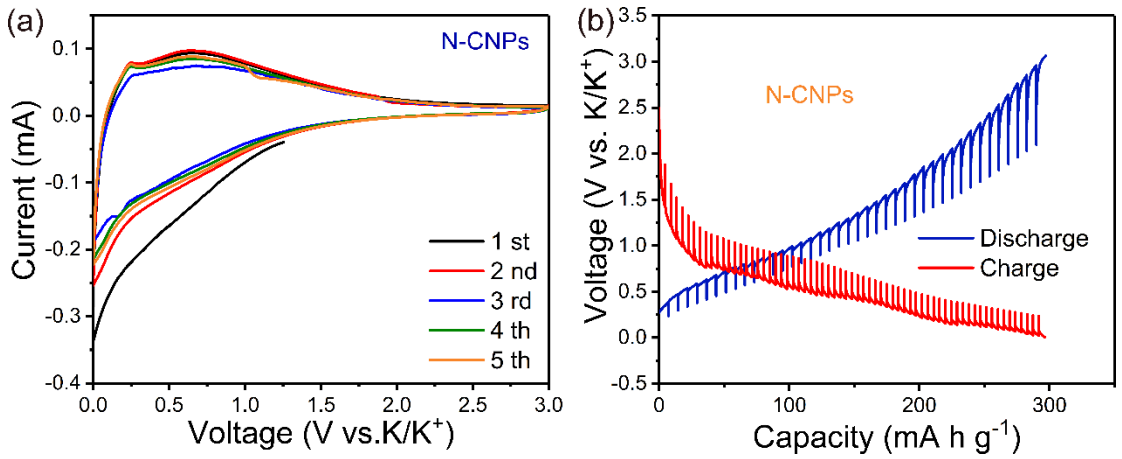

Figure S9. (a) CVs of the initial five cycles at 0.2 mV s^{-1} of N-CNPs. (b) GITT potential profiles for P-CNPs.

The diffusion coefficient (D) in N-CNPs and NP-CNPs electrodes can be calculated from the GITT potential profiles through Fick's second law according to the following equation S1:

$$D = \frac{4}{\pi\tau}\left(\frac{m_B V_M}{M_B S}\right)^2\left(\frac{\Delta E_s}{\Delta E_t}\right)^2$$

where τ represents the duration of the current pulse, m_B stands for the electrode active material mass, S is the geometric area of the electrode, ΔE_s represents the quasi-thermodynamic equilibrium potential difference before and after the current pulse, ΔE_t is the potential difference during current pulse, V_M is the molar volume of the samples, and $M_B$is the molar mass of carbon. The result of M_B/V_M can be calculated from the density of the carbon material based on the following equation S2:

$$\rho = \frac{1}{V_{total} + \frac{1}{\rho_{carbon}}}$$

where ρ (g cm^{-3}) represents the density of the carbon material, V_{total} (cm^3 g^{-1}) represents the total pore volume which comes from the N_2 absorption/desorption isotherms, ρ_{carbon} represents the known true density of carbon (2 g cm^{-3}).

Table S1. Impedance parameters of the fitting equivalent circuit.

Materials		R_e [Ω cm^{-2}]	$R_{(sf+ct)}$ [Ω cm^{-2}]	CPE_i [S $s^{1/2}$ cm^{-2}]	Z_w [S $s^{1/2}$ cm^{-2}]	C_{int} [F cm^{-2}]
N-CNPs	Results	4.875	475	1.07×10^{-4}	0.402	0.0740
	Error (%)	0.964	0.963	2.212	1.242	5.158
NP-CNPs	Results	2.244	188	6.562×10^{-5}	0.419	0.00321
	Error (%)	3.871	2.147	5.838	1.007	4.678

Table S2. Summary of the electrochemical performance of the reported carbon-based anodes for PIBs.

Materials	**Low-rate capacity (mA h g^{-1})**	**High-rate capacity (mA h g^{-1})**	**Capacity retention**
Ordered mesoporous carbon[S1]	286 (50 mA g^{-1})	144 (1000 mA g^{-1})	86.2% over 1000 cycles (1000 mA g^{-1})
Nitrogen-doped carbon microsphere[S2]	250 (33.6 mA g^{-1})	156 (5040 mA g^{-1})	Capacities kept on increasing (4000 mA g^{-1})
Activated graphite[S3]	209 (100 mA g^{-1})	30 (1000 mA g^{-1})	75% over 100 cycles (800 mA g^{-1})
Functionalized carbon nanofibers[S4]	220 (28 mA g^{-1})	70 (1395 mA g^{-1})	78.9% over 300 cycles (140 mA g^{-1})
Hard-soft carbon spheres[S5]	250 (28 mA g^{-1})	190 (560 mA g^{-1})	93% over 200 cycles (280 mA g^{-1})
TC1600[S6]	200 (28 mA g^{-1})	72 (558 mA g^{-1})	78% over 200 cycles (140 mA g^{-1})
N-doped porous carbon monolith[S7]	388 (50 mA g^{-1})	199 (2000 mA g^{-1})	76% over 3000 cycles (1000 mA g^{-1})
Hard carbon microspheres[S8]	262 (28 mA g^{-1})	136 (1400 mA g^{-1})	52% over 100 cycles (1400 mA g^{-1})
Expanded graphite[S9]	263 (10 mA g^{-1})	175 (200 mA g^{-1})	Capacities kept on increasing (200 mA g^{-1})
porous CNF anodes[S10]	250 (20 mA g^{-1})	140 (5000 mA g^{-1})	88% over 1200 cycles (20 mA g^{-1})
NP-CNPs	**400 (50 mA g^{-1})**	**157 (5000 mA g^{-1})**	**86.4% over 4000 cycles (1000 mA g^{-1})**

References

(S1) Wang, W.; Zhou, J.; Wang, Z.; Zhao, L.; Li, P.; Yang, Y.; Yang, C.; Huang, H.; Guo, S. Short-Range Order in Mesoporous Carbon Boosts Potassium-Ion Battery Performance. *Adv. Energy Mater.* **2017**, *8*, 1701648.

(S2) Chen, C.; Wang, Z.; Zhang, B.; Miao, L.; Cai, J.; Peng, L.; Huang, Y.; Jiang, J.; Huang, Y.; Zhang, L.; Xie, J. Nitrogen-Rich Hard Carbon as A Highly Durable Anode for High-Power Potassium-Ion Batteries. *Energy Storage Materials* **2017**, *8*, 161-168.

(S3) Tai, Z.; Zhang, Q.; Liu, Y.; Liu, H.; Dou, S. Activated Carbon from the Graphite with Increased Rate Capability for the Potassium Ion Battery. *Carbon* **2017**, *123*, 54-61.

(S4) Adams, R. A.; Syu, J. M.; Zhao, Y.; Lo, C. T.; Varma, A.; Pol, V. G. Binder-Free N- and O-Rich Carbon Nanofiber Anodes for Long Cycle Life K-Ion Batteries. *ACS Appl. Mater. Interfaces* **2017**, *9*, 17872-17881.

(S5) Jian, Z.; Hwang, S.; Li, Z.; Hernandez, A. S.; Wang, X.; Xing, Z.; Su, D.; Ji, X. Hard-Soft Composite Carbon as A Long-Cycling and High-Rate Anode for Potassium-Ion Batteries. *Adv. Funct. Mater.* **2017**, *27*, 1700324.

(S6) Li, Y.; Adams, R. A.; Arora, A.; Pol, V. G.; Levine, A. M.; Lee, R. J.; Akato, K.; Naskar, A. K.; Paranthaman, M. P. Sustainable Potassium-Ion Battery Anodes Derived from Waste-Tire Rubber. *J. Electrochem. Soc.* **2017**, *164*, A1234-A1238.

(S7) Xie, Y.; Chen, Y.; Liu, L.; Tao, P.; Fan, M.; Xu, N.; Shen, X.; Yan, C. Ultra-High Pyridinic N-Doped Porous Carbon Monolith Enabling High-Capacity K-Ion Battery Anodes for Both Half-Cell and Full-Cell Applications. *Adv. Mater.* **2017**, *29*, 1702268.

(S8) Jian, Z.; Xing, Z.; Bommier, C.; Li, Z.; Ji, X. Hard Carbon Microspheres: Potassium-Ion Anode Versus Sodium-Ion Anode. *Adv. Energy Mater.* **2016**, *6*, 1501874.

(S9) An, Y.; Fei, H.; Zeng, G.; Ci, L.; Xi, B.; Xiong, S.; Feng, J. Commercial Expanded Graphite as A Low-Cost, Long-Cycling Life Anode for Potassium-Ion Batteries with Conventional Carbonate Electrolyte. *J. Power Sources* **2018**, *378*, 66-72.

(S10) Zhao, X.; Xiong, P.; Meng, J.; Liang, Y.; Wang, J.; Xu, Y. High Rate and Long Cycle Life Porous Carbon Nanofiber Paper Anodes for Potassium-Ion Batteries. *J. Mater. Chem. A* **2017**, *5*, 19237-19244.